Segmentation of Gray Scale Images of Dropwise Condensation on Textured Surfaces

Helene Martin, Solmaz Boroomandi Barati, Jean-Charles Pinoli, Stephane Valette, Yann Gavet

Abstract—In the present work we developed an image processing algorithm to measure water droplets characteristics during dropwise condensation on pillared surfaces. The main problem in this process is the similarity between shape and size of water droplets and the pillars. The developed method divides droplets into four main groups based on their size and applies the corresponding algorithm to segment each group. These algorithms generate binary images of droplets based on both their geometrical and intensity properties. The information related to droplets evolution during time including mean radius and drops number per unit area are then extracted from the binary images. The developed image processing algorithm is verified using manual detection and applied to two different sets of images corresponding to two kinds of pillared surfaces.

Keywords—Dropwise condensation, textured surface, image processing, watershed.

I. INTRODUCTION

DROPWISE condensation attracted lots of attention in many industrial applications since about 80 years ago [1] due to its high rate of heat transfer [2]. Though this phenomenon is not preferred in optical applications, for example in automotive industry the light passing through car headlights distracts by water droplets generated during dropwise condensation.

Generally condensation occurs when the temperature of saturated air goes behind its dew point [3]. In this case, water droplets start to nucleate either in the air mixture or on the cold substrate of chamber walls. Regarding condensation on cold substrate, nucleation can occur homogeneously (when there is no preference between different spots for nucleation) or heterogeneously (preferentially on the surface imperfections) [4]. In both cases, dropwise condensation occurs in four main steps: nucleation, growth of droplets by adsorbing water molecule, coalescence and steady state. In the last step, a constant pattern in both the size and number of droplets is visible [5].

Heterogeneous dropwise condensation on textured surfaces is now more attractive to scientists because of the ability of controlling droplets configuration [6]. This idea could also be interesting for optical applications. Indeed, this solution could make drops to form a continuous film or to drain quickly from the surface of headlights or glasses. Thus, several techniques were developed in order to study the characteristics and the evolution of droplets on textured surfaces. The first step of all these methods is the image processing techniques that extract all droplets information from gray scale images. These techniques deal with non intrusive methods with a high spatial and temporal resolution [7].

Most of the time, such image processing algorithms are divided into three main steps: pre-processing, drop segmentation and drop reconstruction. The first one aims at improving contrast and removing noise in order to facilitate the drop segmentation step. The drop segmentation step consists of isolating drops from the background and then separating overlapping drops. The corresponding algorithms can be classified into three groups: the ones based on the shape analysis, based on the edge analysis, and based on the intensity analysis. The algorithms based on the shape analysis consider drops as circles with dark edges and bright centers. These drops can be detected by using circle detection methods like the Hough transform [8] and its improvements, such as the normal-line Hough transform [9] and the coherent circle Hough transform [10]. However, these methods are only efficient for spherical droplets. The algorithms based on the edge analysis use images generated by an edge detection method [11]. For this purpose, the Canny method seems to be the most convenient since although it is more sensitive to noise with respect to other methods, it provides more connected contours. Then the contour discontinuities that represent multiple drops overlapping are detected. such points are called breakpoints, that can be detected by means of several techniques, either by rotating the edge curves [12] or by analyzing their curvature [13], [14]. The main drawback of these techniques is the noise sensitivity, which necessitates to smooth the edge curvatures. A way to limit the noise sensitivity of measurements is to use an adaptive curvature [15]. Finally, the algorithms based on an intensity analysis use the gray-level intensities as a drop presence indicator. These intensities can be used directly like the PIV methods [16] using a dynamic thresholding and watershed [17] or indirectly like the appearance-based approaches using an isolated drop to select the same appearance drops [18]. These methods can be combined thorough a tree of decision to improve the detection quality [7]. For instance, the PIV methods are particularly efficient for isolated drops while the watershed method works well for overlapping ones. However, this combination requires a long computational time.

The drop reconstruction step consists of reconstructing

H. Martin is with Ecole Nationale Suprieure des Mines de Saint-Etienne, LGF UMR CNRS 5307, SAINT-ETIENNE, France.

S. Boroomandi Barati is with Univ Lyon, Ecole Nationale Suprieure des Mines de Saint-Etienne, LGF UMR CNRS 5307, SAINT-ETIENNE, France (e-mail: solmaz.boroomandi@emse.fr).

J.-C. Pinoli is with Ecole Nationale Suprieure des Mines de Saint-Etienne, LGF UMR CNRS 5307, SAINT-ETIENNE, France.

S. Valette is with Univ Lyon, Ecole Centrale de Lyon, LTDS UMR CNRS 5513, F-69134, LYON, France.

Y. Gavet is with Ecole Nationale Suprieure des Mines de Saint-Etienne, LGF UMR CNRS 5307, SAINT-ETIENNE, France.

World Academy of Science, Engineering and Technology
International Journal of Computer and Information Engineering
Vol:12, No:9, 2018

missing parts of drops by determining their radius and their centers. These methods can be divided into four main groups: the ones based on ellipse fitting, based on the geometrical analysis, based on the morphological analysis and the ones using drop inner boundaries. The ellipse fitting methods consist of recognizing ellipse-like shapes in the image. For this purpose, least-squares fitting methods [19] or k-means methods [20] are used. However, these methods work only on ellipsoidal droplets. The geometrical methods aim at determining whether two arcs belong to the same drops by means of either correlation coefficients [12] or applying convexity criteria directly to the contour image [21] or to the polygonal approximation image [22]. The main drawback of these methods is the use of deterministic parameters. The morphological techniques use the morphological reconstruction principle. For this purpose, overlapping drops are reduced to independent characteristic areas before being reconstructed, but the percentage of overlapping droplets must not be too high. Different techniques can be used in this regard: successive erosion [23], [24], skeletonization and shrinking [25] or the watershed technique applied to a distance map [26]. After all, a final technique is applied in order to complete missing parts of droplets by using drops inner boundaries [7]. This last method necessitates high inner boundaries quality.

However, in the case of textured surfaces, the pillars which represent the texturation do not let one to use directly these techniques, although they are adapted to different drop shapes and image conditions. Indeed, pillars have the same properties as drops, they have dark edges and bright centers. Moreover, when the drop shape becomes irregularly connected over the pillars, the already-existing methods are not able to separate them and recognize each droplet. Thus, the goal of this work is to find a way to detect separately drops and pillars in order to analyze drop characteristics evolution on the surface.

This work consists of finding an automatic way to segment drops on several textured surfaces in order to study droplets characteristics. In the following, the experimental set-up enabling to photograph textured surface under dropwise condensation condition will be described. Then, the details of the developed image processing algorithm will be presented. Finally, the algorithm accuracy will be determined and the measurement results will be discussed.

II. EXPERIMENTAL SET-UP

The schematic of the experimental set-up is shown in Fig. 1. The textured substrate with temperature 281K is placed inside a humid chamber with relative humidity of about 40% and air temperature of 303K. The humid air is generated by mixing filtered compressed air and saturated air.

Dropwise condensation on the sample is recorded by a CCD gray scale camera at each second. This camera uses a long-focal-distance adjustable lens in order to get a high spatial resolution. The gray-level images are then used in the following image processing algorithm.
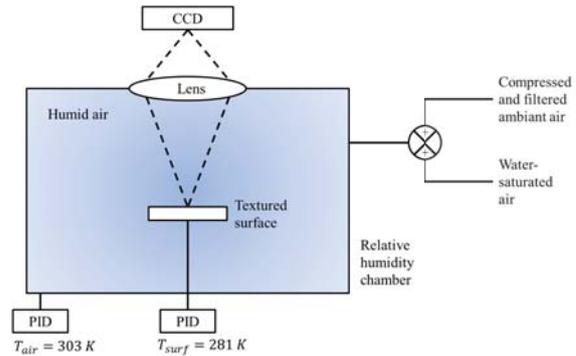

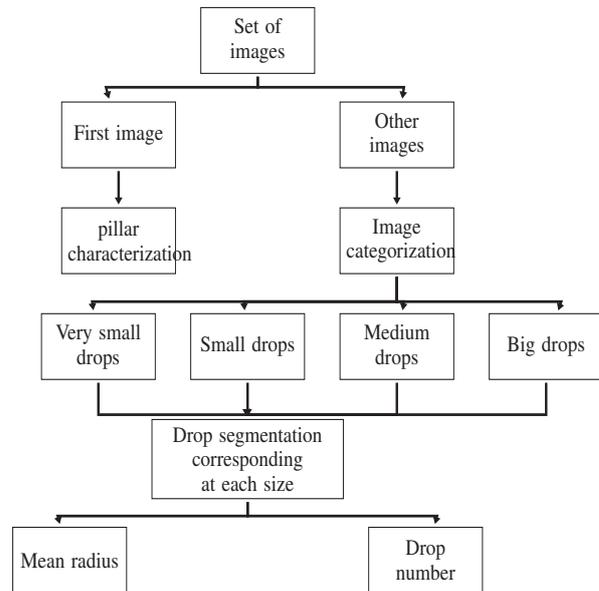
Fig. 1 Schematic of the experimental set-up

Fig. 2 Schematic diagram of the image processing algorithm

III. IMAGE PROCESSING ALGORITHM

An image processing algorithm has been developed to segment drops and to analyze drop characteristic evolution during dropwise condensation. This algorithm is applied to a set of images and it consists of three main steps as shown in Fig. 2. The pillar characterization step aims at isolating pillars in order to remove them from the other images. The goal of the second step is to divide the image set into several groups: very small drops, small drops, medium drops and big drops. The first two groups refer to the drop growth by adsorption. The third group corresponds to the coalescence step and the last one corresponds to the steady state where the changes in size and number of droplets are negligible. After this categorization, the corresponding image processing algorithm is applied to each group. Thus, an image of drop segmentation is generated on which the mean radius and drop number can be measured.

A. Pillar Characterization

The goal of this step is to isolate pillars from background in order to remove them in the other images. In fact, pillars can

World Academy of Science, Engineering and Technology
International Journal of Computer and Information Engineering
Vol:12, No:9, 2018

entail mis-measurement because of their similar properties to drops. As the images are taken without shifting, pillars are at the same location on the images from the same set. So for the purpose of pillar elimination, the first image of the considering set is used because the drop presence can be neglected. The algorithm is detailed in Fig. 3.

As pillars are perfectly circular, the circle Hough transform is the most adapted technique. Moreover, an approximation of pillar radius is known. Indeed, their real size is between 10 and 20 μm and according to the camera magnification, the radius range considered for the Hough transform is [10; 30] pixels. It is important to consider a quite narrow range in order to get accurate results and a low computational time. To improve again the algorithm performances, the coherent Hough transform is used [10].

By means of this method, all the pillars are detected except the ones at the image borders. However, some artefacts are detected too as shown in Fig. 3 (b). As they don't have the same size as pillars, a technique to solve this problem is to consider the distribution of circle radius and to remove the ones with an aberrant radius, as shown in Figs. 3 (c) and (d). Thus, the circle radius must be inside the band [μ - 3.9 σ; μ + 3.9 σ] to be considered as pillars, where μ and σ are the average and the standard deviation of the radius distribution.

At the same time, a manual pillar recognition test is led, as shown in Fig. 3 (e). This secondary method enables to confirm the position of pillars and to validate the calculated radius. Indeed, if the radius are smaller than the real ones, the pillar boundaries will not be taken into account and they will be considered as pillars during the drop segmentation step. Similarly, if the radius are wider than the real ones, some drops will be removed.

Fig. 3 (f) shows that pillars from the Hough transform are lightly smaller than the real ones, that can be explained by their blurred boundaries. Consequently, the circles from the Hough transform must be enlarged. In order to quantify the correct radius, the equivalent circle radius is calculated by means of the manual measurements. This equivalent radius refers to the radius of the circle with the same center as the one from the Hough transform but covering both the Hough transform circle and the manual measured circle, as shown in Fig. 4. In our case, pillar radius must be enlarged from four-pixel wide.

Finally, the binary image of the pillars is generated. The image with the radius from the Hough transform is firstly generated and then, the image is dilated by a disk structuring element, whose radius corresponds to circle enlargement found previously. The final results show visually good approximation of the pillar location and dimension.

It is important to note that the pillars close to the image borders can't be detected because the missing parts are too large. Thus, this problem must be taken into account in the next parts of the algorithm. For instance, the images will be resized.

B. Image Categorization

As mentioned previously, there are four kinds of drops: very small drops, small drops, medium drops and big drops.

It is important to distinguish these groups because the drop identification algorithm will be adapted to each kinds of drops.

This step is like a texturation determination process. Two main categorization methods exist: the ones based on the intensity distribution [27] and the ones based on the pattern distribution [28], [29]. As the image categorization needs to be very fast, the study of intensity histograms is more preferred in our case.

Firstly, a sub-sampling of the image set is done to limit the computational time. Thus, ten percent of images have been chosen regularly, since the time step between images is equal to 1s, 10% of images means the images have been taken after each 10s. The corresponding gray-tone level histograms of each studied image is determined. As shown in Fig. 5, the number of major peaks in histograms vary as a function of time. This variation represents the different drop sizes. Thus, the ranges of each size group of drops are characterized:

- Very small drops: histogram with three major peaks, corresponding to the background, the drop edge and the drop center.
- Small drops: after a while when the histogram of gray tone turns in to bimodal diagram, the majority of droplets are called small droplets that grow mainly due to adsorption. With respect to the former stage here the peak related to the background disappeared because drops tend to cover entirely the sample.
- Medium drops: In the third stage, drops start to coalesce and their centers become larger with the same intensity as background. Therefore the gray tone histogram will turn to a unimodal diagram. The droplets at this stage are so called medium drops.
- Big drops: Finally, when the droplets are big enough to reach the steady state condition, the gray tone histogram will have two peaks again, that refer to the drop edges and centers.

C. Drop Identification

This last part of the algorithm consists of identifying drops in each image during dropwise condensation in order to determine the evolution of drop characteristics.

1) Very Small Drops: The very small drops refer to the small elements between pillars (Fig. 6). The idea of this algorithm is to segment drops by means of correct thresholding values, as shown in Fig. 7.

At first, in order to eliminating the pillars, they are removed by means of the image generated in the pillar characterization step. Thus, a gray-level image is obtained with black holes at pillar places, as shown in Figs. 7 (a) and (b). Fig. 7 (c) shows the histogram corresponding to the images containing very small droplets. This process is applied in parallel to the first image at time of zero (Figs. 7 (d)-(f)).

The very small droplets spread the gray tone histogram towards darker area, because generally they are darker than the substrate. Therefore, the superposition point between these two histograms can be used as thresholding value for Fig. 7 (a). But since there are lots of superposition points between these two histograms along the vertical axis, the thresholding

World Academy of Science, Engineering and Technology
International Journal of Computer and Information Engineering
Vol:12, No:9, 2018

(b) Hough transform   (c) Artefact detection   (d) Artefact removing

(a) Original image   (e) Manual detection   (f) pillar comparison
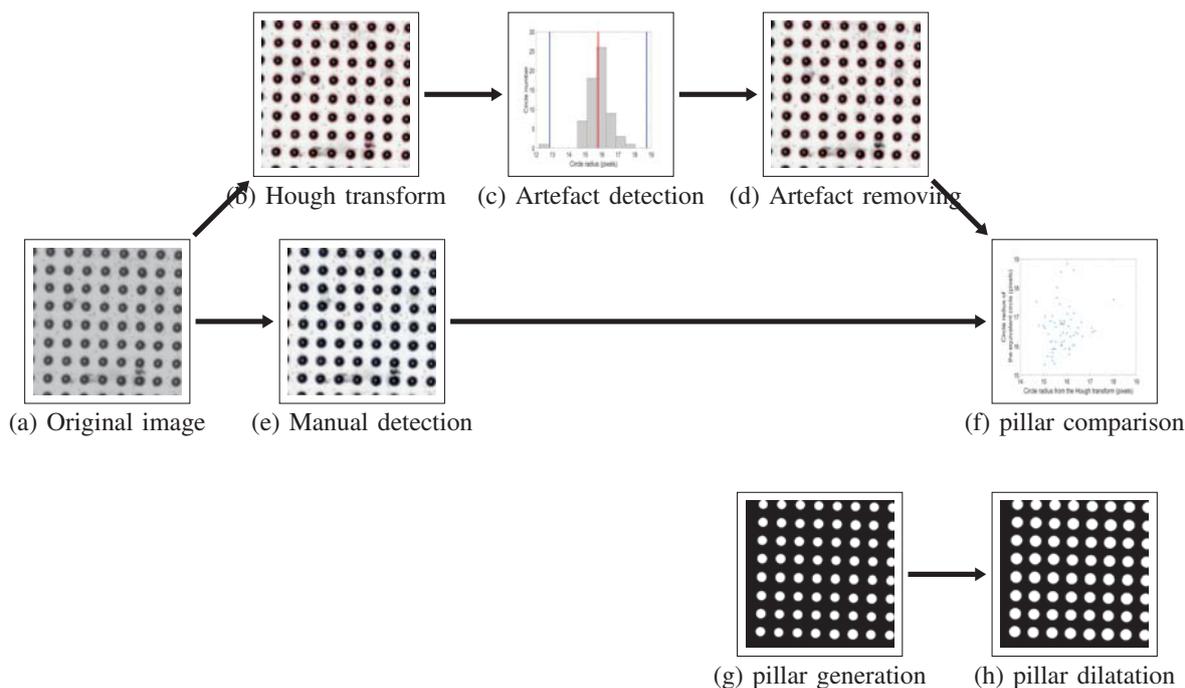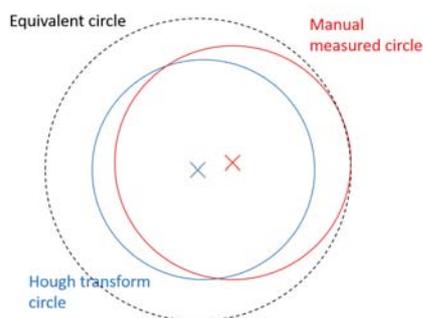
(g) pillar generation   (h) pillar dilatation

Fig. 3 Algorithm for pillar characterization

Fig. 4 Equivalent circle determination
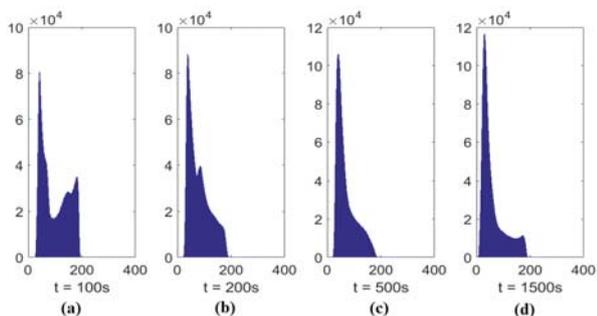
Fig. 5 Intensity histogram of (a) very small droplets at $t = 100s$, (b) small droplets at $t = 200s$, (c) medium droplets at $t = 500s$ and (d) big droplets drops at $t = 1500s$
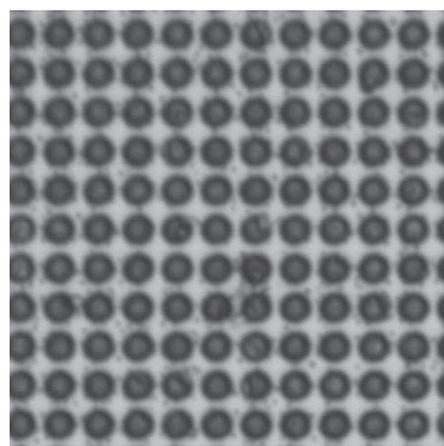

Fig. 6 Image of very small drops on a textured surface

peak corresponds to the maximum superposition point or the thresholding value. This value then used for thresholding the images containing very small drops as is shown in Fig. 7 (h). At last each region is labeled according to Fig. 7 (i). Therefore, the number of regions corresponds to the drop number N, that enables to determine the mean drop radius R_{avg} from the total region area A:

$$R_{avg} = \sqrt{\frac{A_{tot}}{N\pi}}. \qquad (1)$$

2) Small Drops: Small drops are presented as small circular elements which are smaller than the pillars in the images (Fig. 8). Since, at this step, droplets are perfectly circular, they can be recognized by means of the Hough transform as shown in

value can be calculated by finding the superposition point with the maximum value. Fig. 7 (g) represents the difference between these two histograms and the zero values in this graph shows the superposition points. So the first zero point after the

World Academy of Science, Engineering and Technology
International Journal of Computer and Information Engineering
Vol:12, No:9, 2018

(a) Original image   (b) pillar removing   (c) Histogram

(g) Thresholding value   (h) Thresholding

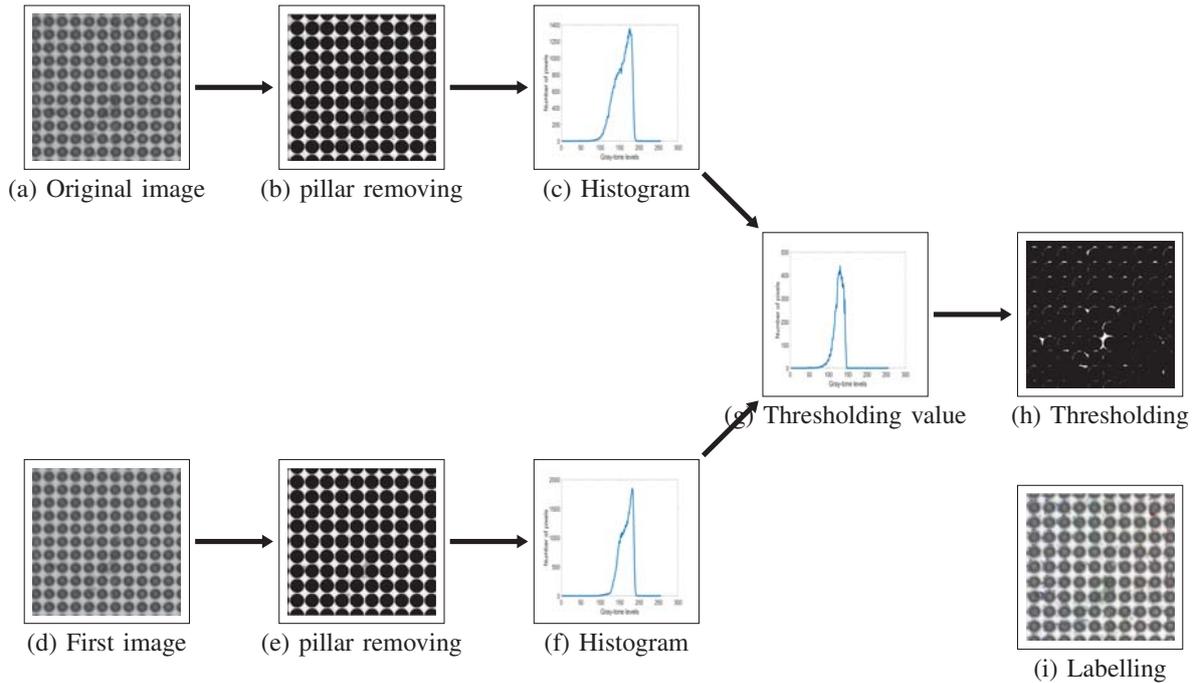(d) First image   (e) pillar removing   (f) Histogram

(i) Labelling

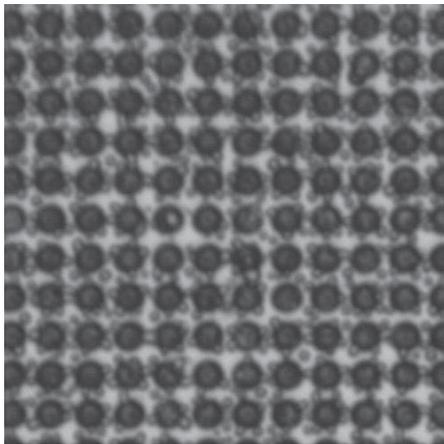Fig. 7 Algorithm for very small drops

Fig. 9 (b).

Fig. 8 Image of small drops on a textured surface

Then, as shown in Fig. 9 (c), the circles corresponding to pillars are removed by comparing the position of circle centers between the considered image and the first image of the set. A binary image is obtained (Fig. 9 (d)), it gives the total area A_{tot} of drops. To get the number of drops, the overlapping drops need to be separated. For this purpose, the binary image is turned into a distance map by the Euclidean distance (Fig. 9 (e)) and the watershed technique is applied to this distance map (Fig. 9 (f)). A labeling step enables to get the drop number and finally, the equation 1 gives the mean radius of drops.

3) Medium Drops: The medium drops form a continuous cluster around pillars and drop centers look like background regions (Fig. 10). Therefore, the centers of drops must be determined by means of some criteria based on both geometry and intensity (Fig. 11).

In this regard, the original images are firstly thresholded by means of Otsu's method as is shown in Fig. 11 (b). The problem here is that white area represents both droplets center and substrate. In order to recognising droplets center, two techniques are applied to sufficiently large white regions. The droplets centers are either more convex than substrate or are less homogeneous in intensity. Consequently, the areas with the convexity rate under 4 % (Fig. 11 (d)) or with low rate of gradient magnitude refer to the drops centers (Fig. 11 (c)). The limited rate of gradient magnitude corresponds to 4/5 of the mean gradient magnitude of the neighborhoods. Finally, the binary images of drops as in Fig. 11 (f) are made by applying the watershed method.

4) Big Drops: Big drops are characterized by the fact that they cover entirely several pillars as shown in Fig. 12. For binarizing images containing big droplets, shrinking and gradient properties are used (Fig. 13).

Firstly, the images are thresholded by a Otsu's method as shown in Fig. 13 (b). Then, the black parts are shrunk in order to get their skeletons (Fig. 13 (c)) around the white regions which correspond to either drops centers or the background. As was explained for the medium drops, the average of gradient magnitude is calculated on the white regions according to Fig. 13 (d). Then, the distribution of this value is divided into two groups by means of the histogram specification, the median between the two main peaks, that gives the criterion value (Fig. 13 (e)).

However, when several white regions belong to the same drop, the watershed technique can't be applied directly. To solve this problem, the white regions are dilated and overlaid
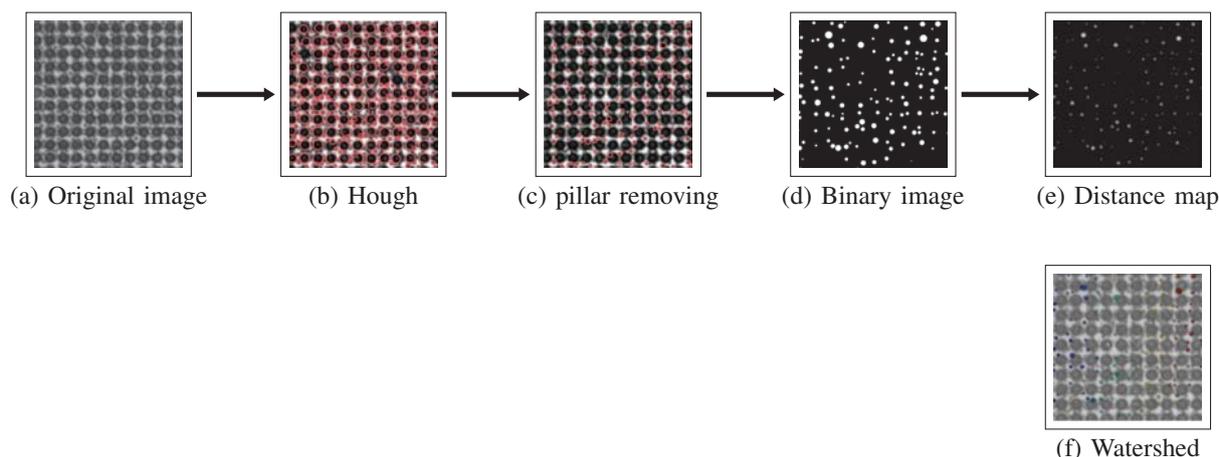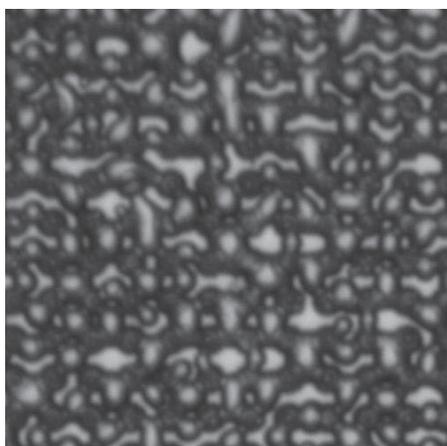
World Academy of Science, Engineering and Technology
International Journal of Computer and Information Engineering
Vol:12, No:9, 2018

(a) Original image　　(b) Hough　　(c) pillar removing　　(d) Binary image　　(e) Distance map

(f) Watershed

Fig. 9 Algorithm for small drops

Fig. 10 Image of medium drops on a textured image

TABLE I
PERFORMANCE PARAMETERS OF THE ALGORITHM FOR SEVERAL IMAGE SETS

Set	Drop size	FM
Regular pattern	Very small	75 %
	Small	49 %
	Medium	84 %
	Big	93 %
Quincunx	Very small	-
	Small	5 %
	Medium	71 %
	Big	87 %

algorithm:

$$PR = \frac{TP}{TP + FP}, \qquad (2)$$

$$RC = \frac{TP}{TP + FN}. \qquad (3)$$

A high value of PR indicates that detected drops are present in the original image and there can be other drops which are not detected by the algorithm. On the contrary, a high value of RC indicates that the algorithm detects almost all drops, but it also detects some drops, which do not exist in the original image. Thus, these both measurements suffer from a lack of accuracy. In fact, neither FN nor FP are not preferred for an accurate algorithm. That's why, a more robust measurement of the algorithm accuracy so-called F-measure (FM) is used [30]:

$$FM = \frac{2}{1/PR + 1/RC}. \qquad (4)$$

In order to evaluate the F-measure of this algorithm, the drops are manually detected in a sub-sampling of images and are compared with those detected by means of the algorithm. This study is led to two kinds of surfaces (grid pattern and quincunx pattern) in order to determine the application conditions of the algorithm. Table I shows the evolution of the F-measure as a function of the considered image set and the drop size.

The low values obtained for small drops can be explained by the fact that drops are not really circular because they are adjacent to pillars. Despite these mis-measurements, Table I shows that this algorithm is very accurate, especially for

with the pillar image. Thus, the white regions which belong to the same drop are connected. A test on convexity enables to reconstruct each drop center (Fig. 13 (g)). Finally, a watershed technique is used to detect each drop region (Fig. 13 (h)), that enables to get the drops number and mean radius.

IV. ALGORITHM VERIFICATION

In order to measure quantitatively the performance of this algorithm, the drops are divided into four groups according to their presence in the initial configuration and their detection by the algorithm:

- The true positive drops (TP) which are detected by the algorithm and are present in the initial image.
- The false positive drops (FP) which are detected by the algorithm but are not present in the initial image.
- The false negative drops (FN) which are not detected by the algorithm but are present in the initial image.
- The true negative drops (TN) which are not detected by the algorithm and are not present in the original image.

The number of drops which belong to each groups enables to estimate the precision (PR) and the recall (RC) of the

World Academy of Science, Engineering and Technology
International Journal of Computer and Information Engineering
Vol:12, No:9, 2018

(c) Low gradient parts

(a) Original image   (b) Thresholding   (e) Drop centers   (f) Watershed
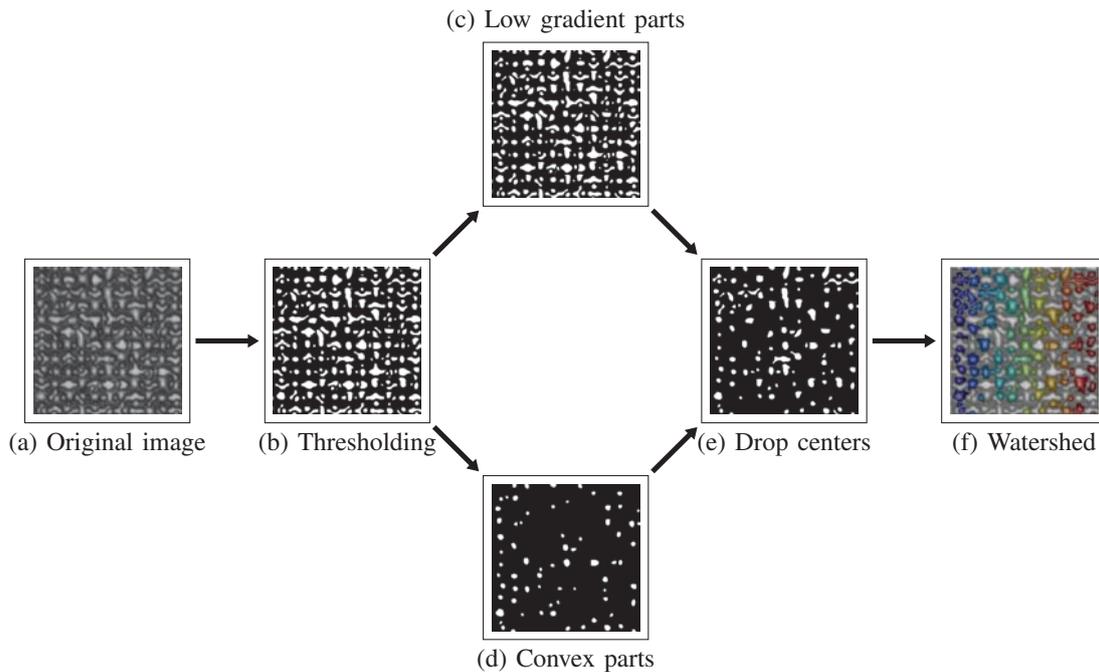
(d) Convex parts
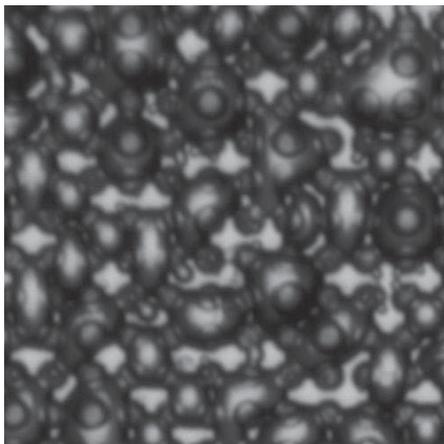
Fig. 11 Algorithm for medium drops

Fig. 12 Image of big drops on a textured image

large drops. Although the detection on the quincunx pattern is less accurate. Thus, the pillar pattern has an influence on the algorithm accuracy.

V. APPLICATION TO TEXTURED SURFACES

The developed image processing algorithm is applied to images generated by the experimental set-up described in Section II. Several texturation are tested: grid pattern and quincunx pattern.

Fig. 14 shows the evolution of the drop mean radius during dropwise condensation for both textured surfaces. The measurements were done every $10s$ in order to reduce the computational time. As can be seen in this figure, the drops mean radius increases to reach a steady state situation, that

follows the theory of dropwise condensation: droplets grow and coalesce until reaching a regular pattern [5].

Fig. 15 shows the evolution of the drop number during dropwise condensation for both of the textured surfaces. In both cases, the drops number decreases rapidly to reach a steady state situation, after which the number of droplets follow a constant pattern.

The steady state situation in both radius and number of droplets is due to coalescence phase, during which two or more small droplets merge and form a bigger droplet. This phenomenon leads to decrease in the total surface area covered by the droplets, In the vacant area formed after coalescence new small droplets can nucleate continuously. The opposite effect of coalescence and nucleation of new small droplets on the average size and total number of droplets will lead to an approximately constant pattern in these two diagrams.

However, the fluctuations at the initial seconds of the algorithm show the lack of robustness of this algorithm in initial stages of dropwise condensation.

The comparison between droplets radius and density between two kinds of texturation reveals that, the drops mean radius for the quinqunx pattern is lower than the one for the grid pattern. In parallel, the initial droplets density for the grid pattern is higher than quinqunx pattern. While for both texturations, these measurements reach the same values at steady state: $0.25mft$ for the mean radius and $301/ft^2$.

Figs. 16 and 17 compare the drop characteristics of the grid patterned surface with a flat surface formed with the same material in order to see the influence of pillars on the drop evolution. According to Fig. 16, the presence of the pillars limits the increasing of drop radius at steady state of about 50%. However, during other steps, droplets on the flat surface

World Academy of Science, Engineering and Technology
International Journal of Computer and Information Engineering
Vol:12, No:9, 2018

(a) Original image (b) Thresholding (c) Shrinking (d) Low gradient parts (e) Gradient histogram

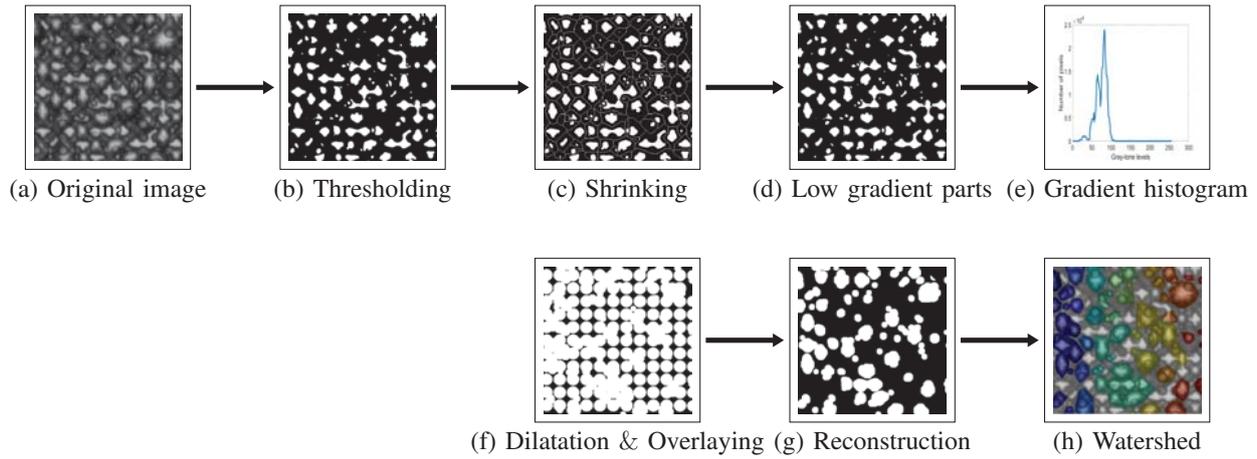(f) Dilatation & Overlaying (g) Reconstruction (h) Watershed
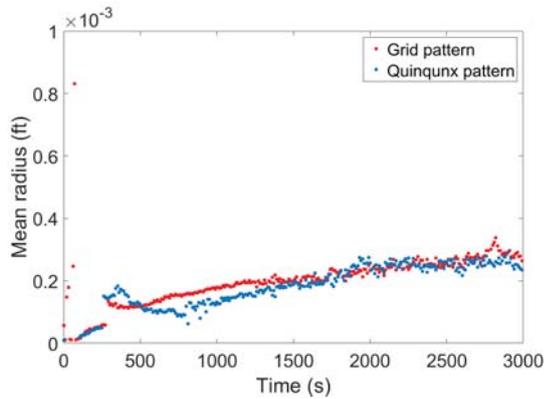
Fig. 13 Algorithm for big drops

Fig. 14 Evolution of the mean radius as a function of time for two kinds of
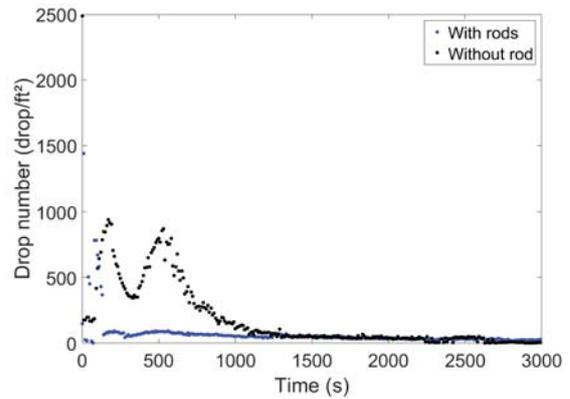texturation

Fig. 16 Comparison of the mean radius evolution for a grid patterned
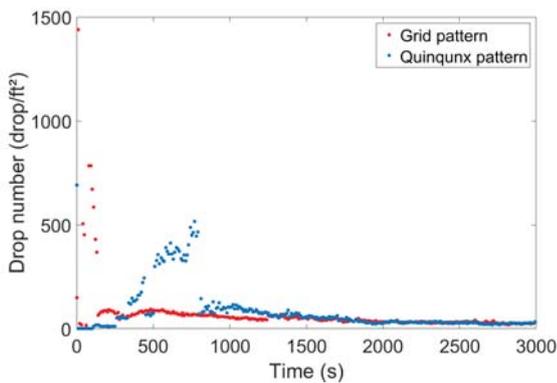surface and a flat surface

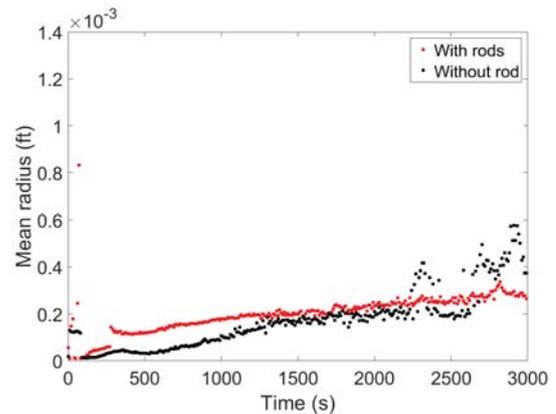Fig. 15 Evolution of the drops number as a function of time for two kinds
of texturation

Fig. 17 Comparison of the drop number evolution for a grid patterned
surface and a flat surface

are respectively larger. On the other hand, the presence of
pillars increases considerably the drops number during the
initial steps.

VI. CONCLUSION

A robust image processing algorithm has been developed
for drop measurement on textured surfaces. The existing
techniques of drop measurement have been discussed and have
been proved to be adequate in the case of pillar texturation

World Academy of Science, Engineering and Technology
International Journal of Computer and Information Engineering
Vol:12, No:9, 2018

too. Thus, the developed algorithm combines the geometrical, optical and topological information of the images to segment the droplets. It is capable of segmenting drops with a large range of radius. Indeed, by means of an histogram analysis, it can estimate the drop size, divides the drops in four main size range and uses a corresponding algorithm adapted to each size range. A manual verification of drop detection ability of the present algorithm comparing to real images is conducted to verify the algorithm accuracy. The F-measure enables to quantify the accuracy of the detection and to show that this algorithm has a high accuracy for drops with a radius over $0.15 m f t$.

The developed algorithm gives the evolution of drops mean radius and number per unit area during dropwise condensation. It has been applied to two kinds of textured surfaces in order to compare the wettability of each texturation. This comparison shows that the texturation pattern affects the droplets size and the density before steady state situation. The comparison with flat surface shows that, although texturation enables to reduce the droplets size at later stages, it increases the density of initial nucleation.

ACKNOWLEDGMENT

REFERENCES

[1] R. N. Leach, F. Stevens, and J. T. Dickinson. Dropwise condensation - experiments and simulations of nucleation and growth of water drops in a cooling system. Technical report, Physics Department, Washington State University, 2006.

[2] Y. A. Cengel. Heat transfer - a practical approach. Technical report, International Edition, 1998.

[3] Julian E. Castillo, Justin A. Weibel, and Suresh V. Garimella. The effect of relative humidity on dropwise condensation dynamics. Technical report, Cooling Technologies Research Center, Purdue University, 2015.

[4] R. N. Leach, F. Stevens, S. C. Langford, and J. T. Dickinson. Dropwise condensation: eperiments and simulations of nucleation and growth of water drops in alccoling system. Technical report, Physics Department, Washington State University, 2009.

[5] J. W. Rose and L. R. Glicksman. Dropwise condensation - the distribution of drop sizes. Technical report, Department of Mechanical Engineering, Massachusets Institute of Technology, 1972.

[6] Basant Singh Sikarwar, Sameer Khandekar, and K. Muralidhar. Mathematical modelling of dropwise condensation on textured surfaces. Technical report, Department of Mechanical Engineering, Indian Institute of Technology Kanpur, 2012.

[7] Yucheng Fu and Yang Liu. Development of a robust image processing technique for bubbly flow measurement in a narrow rectangular channel. Technical report, Nuclear Engineering Program, Mechanical Engineering Department, Virginia Tech, 2016.

[8] Soo-Chang Pei and Ji-Hwei Horng. Circular arc detection based on hough transform. Technical report, Department of Electrical Engineering, National Tawan University, 1995.

[9] Xiaoran Yu, Dongchang Xing, Tatsuya Hazuku, Tomoji Takamasa, Takaski Ishimaru, Yuji Tanaka, and Tatsuro Akiba. Measurement technique for solid-liquid two-phase flow using normal-line hough transform method. Technical report, Tokyo University of Marine Science and Technology - Research Institute for Cell Engineering Advanced Industrial Science and Technology, 2009.

[10] T. J. Atherthon and D. J. Kerbyson. Using phase to represent radius in the coherent circle hough transform. Technical report, Department of Computer Science, University of Warwick, 1993.

[11] R. Muthukrishnan and M. Radha. Edge detection technique for image segmentation. Technical report, Department of Statistics, Bharathiar University, 2011.

[12] Liping Shen, Xiangqun Song, Manabu Iguchi, and Fujio Yamamoto. A method for recognizing particles in overlapped particle images. Technical report, Department of Mechanical Engineering, Fukui University - Division of Materials Science and Engineering, Graduate School of Engineering, Hokkado University, 1999.

[13] M. Honkanen. Turbulent multiphase flow measurements with particle image velocimetry: application to bubbly flows. Technical report, Tampere University of Technology, 2002.

[14] Herbert Freeman and Larry S. Davis. A corner-finding algorithm for chain-coded curves. Technical report, IEEE Transactions on Computers, 1977.

[15] C. Urdiales, A. Bandera, and F. Sandoval. Non-parametric planar shape representation based on adaptive curvature functions. Technical report, Dpto Technologica Electronica ETSI Telecommunicacion, Universidad de Malaga, 2002.

[16] R. Lindken and W. Merzkirch. A novel piv technique for measurements in multiphase flows and its application to two-phase bubbly flows. Technical report, DHochschule Bochum, Mecatronics and Mechanical Eengineering Department, 2002.

[17] S. Beucher and F. Meyer. The morphological approach to segmentation; the watershed transformation. Technical report, Centre de morphologie mathematique, Ecole des Mines de Paris, 1990.

[18] X. Zabulis, M. Papara, A. Chatziargyriou, and T. D. Karapantsios. Detection of densely dispersed spherical bubbles in digital images based in template matching technique - application to wet foams. Technical report, Division of Chemcal Technology, School of Chemistry, Aristotelian University of Thessaloniki - University Box Informatics and Telematics Institute - Centre for Research and Technology Hellas, 2007.

[19] Andrew W. Fitzgibbon, Maurizio Pilu, and Robert B Fisher. Direct least-squares fitting of ellipses. Technical report, Department of Artificial Intelligence, the University of Edinburgh, 1996.

[20] Tomislav Marosevic and Rudolf Scitovski. Multiple ellipse fitting by center-based clustering. Technical report, Multiple ellipse fitting by center-based clustering, 2015.

[21] A. La Torre, L. Alonso-Nanclares, S. Muelas, J. M. Pena, and J. DeFelipe. Segmentation of neuronal nuclei based on clump splitting and a two-step binarization of images. Technical report, Instituto Cajal, Consejo Superior de Investigaciones - Larboratorio Cajal de Circuitos Corticales and Facultad de Informatica, Universidad Politecnica de Madrid, 2013.

[22] W. X. Wang. Binary image segmentation of aggregates based on polygonal approximation and classification of concavities. Technical report, Dpto Technologica Electronica ETSI Telecommunicacion, Universidad de MalagaDivision of Engineering Geology, Department of Civil and Environmental Engineering, Royal Institute of Technology, 1997.

[23] D. Thompson, H. G. J. W. Haddad, and P. H. Bartels. Scene segmentation in a machine vision system for histopathology. Technical report, Optical Science Center, University of Arizona, 1990.

[24] S. H. Ong and Jayasooriah. Decomposition of digital clumps into convex parts by contour tracing and labelling. Technical report, Optical Science Center, University of ArizonaDepartment of Electrical Engineering, National University of Singapore, 1992.

[25] Ashish Karn, Christopher Ellis, Roger Arndt, and Jiarong Hong. An integrative image measurement technique for dense bubbly flows with a wide size distribution. Technical report, Saint Anthony Falls Laboratory, University of Minnesota, 2015.

[26] Qing Chen, Xiaoli Yang, and Emil M Petrui. Watershed segmentation for binary images with different distance transforms. Technical report, University of Ottawa, Lakehead University, 2004.

[27] R. M. Haralick and L. Waston. A facet model for image data. Technical report, Computer Vision Graphics Image Process, 1981.

[28] Timo Ojala, Matti Pietikinen, and David Harwood. Performance evaluation of texture measures with classification based on kullback discrimination of distributions. Technical report, Department of Electrical Engineering, University of Ouu - Center for Automation Researc, University of Maryland, 1994.

[29] K. L. Lee and L. H. Chen. A new method for coarse classification of textures and class weight estimation for texture retrieva. Technical report, Department of Computer and Information Science, National Chiao Tung University, 2002.

[30] Tom Fawcett. An introduction to roc analysis. Technical report, Institute for the Study of Learning and Expertise, 2005.